

Face Hallucination with Finishing Touches

Yang Zhang, Ivor W. Tsang, Jun Li, Ping Liu, Xiaobo Lu, and Xin Yu

Abstract—Obtaining a high-quality frontal face image from a low-resolution (LR) non-frontal face image is primarily important for many facial analysis applications. However, mainstreams either focus on super-resolving near-frontal LR faces or frontalizing non-frontal high-resolution (HR) faces. It is desirable to perform both tasks seamlessly for daily-life unconstrained face images. In this paper, we present a novel Vivid Face Hallucination Generative Adversarial Network (VividGAN) for simultaneously super-resolving and frontalizing tiny non-frontal face images. VividGAN consists of coarse-level and fine-level Face Hallucination Networks (FHnet) and two discriminators, *i.e.*, Coarse-D and Fine-D. The coarse-level FHnet generates a frontal coarse HR face and then the fine-level FHnet makes use of the facial component appearance prior, *i.e.*, fine-grained facial components, to attain a frontal HR face image with authentic details. In the fine-level FHnet, we also design a facial component-aware module that adopts the facial geometry guidance as clues to accurately align and merge the frontal coarse HR face and prior information. Meanwhile, two-level discriminators are designed to capture both the global outline of a face image as well as detailed facial characteristics. The Coarse-D enforces the coarsely hallucinated faces to be upright and complete while the Fine-D focuses on the fine hallucinated ones for sharper details. Extensive experiments demonstrate that our VividGAN achieves photo-realistic frontal HR faces, reaching superior performance in downstream tasks, *i.e.*, face recognition and expression classification, compared with other state-of-the-art methods.

Index Terms—Face hallucination, super-resolution, face frontalization, generative adversarial network.

I. INTRODUCTION

As the requirement of public security increases, authentication plays an important role in daily life [1]. High-quality face images are one of the most discriminative biometric cues to provide identity verification. However, in most imaging conditions, long distance and relative location between public cameras and human faces are inevitable interference factors, leading to a vast collection of non-frontal tiny face images.

This work was done when the first author visited the University of Technology Sydney. Y. Zhang is with the School of Automation, Southeast University, Nanjing 210096, China; the Australian Artificial Intelligence Institute, University of Technology Sydney, Ultimo, NSW 2007, Australia; the Key Laboratory of Measurement and Control of Complex Systems of Engineering, Ministry of Education, Nanjing 210096, China, e-mail: zhangyang201703@126.com.

I. W. Tsang, J. Li and Xin Yu are with the Australian Artificial Intelligence Institute, University of Technology Sydney, Ultimo, NSW 2007, Australia, e-mail: (ivor.tsang@uts.edu.au, Jun.Li@uts.edu.au, and xin.yu@uts.edu.au).

P. Liu is with the Institute of High Performance Computing, Research Agency for Science, Technology and Research (A*STAR), Singapore 138634 (e-mail: pino.pingliu@gmail.com).

X. B. Lu is with the School of Automation, Southeast University, Nanjing 210096, China; Key Laboratory of Measurement and Control of Complex Systems of Engineering, Ministry of Education, Nanjing 210096, China, email: xblu2013@126.com.

This work was done when Xin Yu was with the Research School of Engineering, Australian National University, Canberra, Australia.

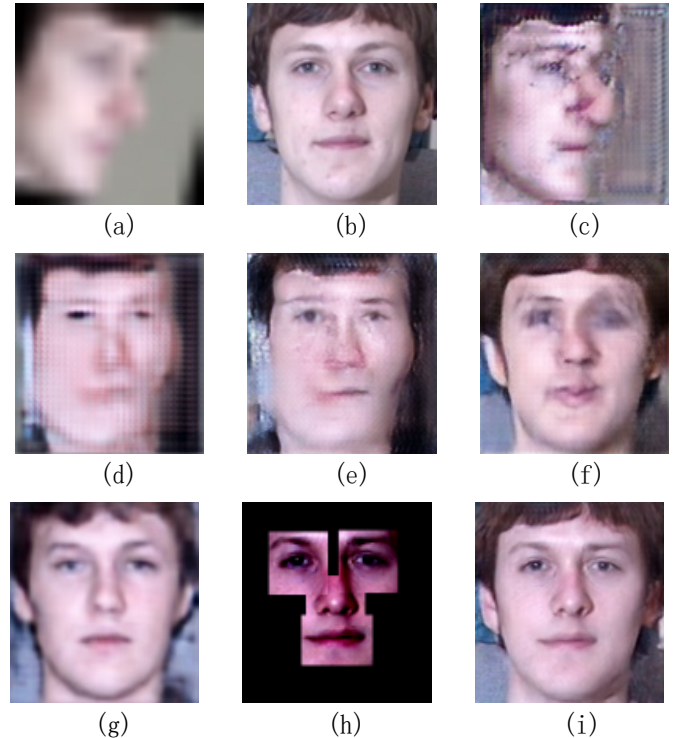


Fig. 1: Face super-resolution and frontalization results on a testing non-frontal LR face. (a) An input non-frontal LR face (16×16 pixels). (b) The ground-truth frontal face (128×128 pixels, not available in training). (c) Result obtained by applying [4] to (a). (d) Face frontalization result of (a) by applying [5] after bicubic upsampling and alignment, where a single STN network [6] is introduced to align (a) first. (e) Result obtained by applying [5] first and then [4]. (f) Result obtained by applying [4] first and then [5]. (g) Result of TANN [7]. (h) Fine-grained facial components. (i) Result of our VividGAN.

Such low-quality face images not only impede human observation but also degrade the performance of downstream machine perception algorithms [2], [3]

Motivated by this challenge, many researchers resort to face super-resolution (SR) techniques to recover high-resolution (HR) face images from the tiny inputs. State-of-the-art face SR methods [4], [8]–[11] utilize deep convolutional neural networks to super-resolve near-frontal low-resolution (LR) faces. Meanwhile, some works [12]–[15] have been proposed to frontalize faces from their non-frontal counterparts. However, those face frontalization techniques [16], [17] mainly warp 2D HR face images based on real-time detected facial landmarks. Hence, they might fail to frontalize very tiny non-frontal faces.

In this work, we aim to hallucinate a frontal HR face from a

non-frontal LR input. A naive idea is to *sequentially* combine existing face SR and frontalization models. However, as seen in Figs. 1(e) and (f), the results undergo obvious distortions and severe artifacts. This is mainly caused by two factors: (i) Both face SR and face frontalization are ill-posed inverse problems, and the errors in either process cannot be eliminated by the other one but are exaggerated. (ii) Pose variations bring challenges to state-of-the-art face SR techniques (see Fig. 1(c)) and low resolution images impose difficulties on existing face frontalization algorithms (see Fig. 1(d)). As a result, we face a chicken-and-egg problem: face SR would be facilitated by face frontalization, while the latter requires an HR face. This challenging issue cannot be addressed by simply combining those two methods.

Very recently, the work [7] proposes a Transformative Adversarial Neural Network (TANN) to jointly frontalize and super-resolve non-frontal LR face images. Unlike the direct combination of face frontalization and SR models, the joint mechanism performed in TANN is able to avoid artifacts. However, since TANN is a single-stage face hallucination network, it does not process a “looking back” mechanism to modify upscaled faces. Therefore, TANN may output blurry facial details under extreme poses or challenging expressions. As visible in Fig. 1(g), unnatural artifacts still exist in the result of TANN.

Different from previous works, we propose a novel Vivid Face Hallucination Generative Adversarial Network (VividGAN). Our VividGAN *jointly* super-resolves and frontalizes tiny non-frontal face images and is designed to *progressively* hallucinate a non-frontal LR face in a coarse-to-fine manner (see Fig. 2), thus reducing unwanted blurriness and artifacts significantly. In this manner, these two tasks, *i.e.*, face SR and frontalization, facilitate each other in a unified framework. Furthermore, we observe that facial components, such as eyes, noses and mouths, are the most distinguishable parts to humans. Therefore, we introduce the facial component appearance prior, *i.e.*, fine-grained facial components, as the semantic guidance to achieve realistic facial details as our “finishing touches”.

Specifically, our VividGAN consists of a Vivid Face Hallucination Network (Vivid-FHnet) that comprises a coarse-level FH network and a fine-level FH network, as well as two discriminators, *i.e.*, Coarse-D and Fine-D. Their details are described as follows:

(i) A coarse-level FH network is designed to super-resolve and frontalize an input non-frontal LR face roughly. We do not assume the input face is aligned in advance. Instead, we interweave the spatial transformation networks (STNs) [6] with upsampling layers to compensate for misalignments. In order to guarantee the content-integrity of hallucinated results, we introduce a mirror symmetry loss based on domain-specific knowledge of human faces. As a result, we can generate coarsely frontal HR faces, which facilitates the next hallucination procedure.

(ii) Subsequently, we propose a fine-level FH network for fine detail recovery of frontal HR face image by explicitly incorporating the facial component appearance prior, *i.e.*, fine-grained facial components. First, we design a touching-up sub-

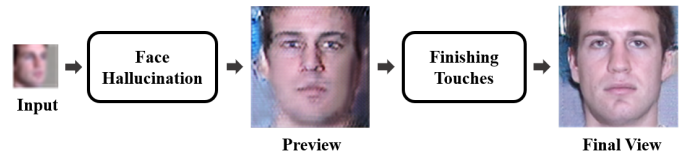


Fig. 2: The pipeline of our VividGAN.

network to effectively estimate the fine-grained facial components by integrating multi-scale upscaling and downsampling blocks (see Fig. 1(h)). Then, we feed the facial component appearance prior and the frontal coarse HR face into a fine-integration subnetwork for further refinement. Particularly, we design a facial component-aware module to align and merge the coarsely restored face and the facial component prior information.

(iii) Different from previous works [7], [18]–[21] that use a single discriminator, we employ two-level discriminators, which promote our coarse-to-fine Vivid-FHnet to produce photo-realistic results. In this fashion, we are able to capture both global outlines and local details of faces. Fig. 1(i) illustrates that our hallucinated frontal HR face is more visually appealing than the results of the state-of-the-art methods.

In summary, our contributions are threefold:

- We propose a novel framework, dubbed Vivid Face Hallucination Generative Adversarial Network (VividGAN), to jointly tackle face SR and face frontalization in a unified framework. In particular, we first upsample and frontalize low-resolution faces in a coarse granularity and then take advantage of facial component appearance priors to remedy the details of coarsely upscaled frontal HR faces.
- We propose a facial component-aware module for face enhancement and alignment. In this way, fine-grained facial components are incorporated into the frontal coarse HR face seamlessly.
- Our experiments demonstrate that VividGAN is able to frontalize and super-resolve (by an upscaling factor of $8\times$) very low-resolution face images (*e.g.*, 16×16) undergoing large poses (*e.g.*, 90°) and complex expressions (*e.g.*, “disgust”, “fear”). Moreover, our VividGAN is also able to provide superior hallucinated face images for downstream tasks, *i.e.*, face recognition and expression classification, in comparison to the state-of-the-art.

II. RELATED WORK

A. Face Super-resolution

Face Super-resolution (SR) aims at establishing the intensity relationships between input LR and output HR face images. The previous works are generally categorized into three main-streams: holistic-based, part-based, and deep learning based methods.

The basic principle of holistic-based techniques is to up-sample a whole LR face by a global face model. Wang *et al.* [22] formulate a linear mapping between LR and HR images to achieve face SR based on an Eigen-transformation of LR faces. Liu *et al.* [23] incorporate a bilateral filtering to mitigate the ghosting artifacts. Kolouri and Rohde [24] morph

HR faces from aligned LR ones based on optimal transport and subspace learning. However, they require LR inputs to be precisely aligned and reference HR faces to exhibit similar canonical poses and natural expressions.

To address pose and expression variations, part-based methods are proposed to make use of exemplar facial patches to upsample local facial regions instead of imposing global constraints. The approaches [25]–[27] super-resolve local LR patches based on a weighted sum of exemplar facial patches in reference HR database. Liu *et al.* [28] develops a locality-constrained bi-layer network to jointly super-resolve LR faces as well as eliminate noise and outliers. Moreover, SIFT flow [29] and facial landmarks [30] are introduced to locate facial components for further super-resolution. Since these techniques need to localize facial components in LR inputs precisely, they may fail to process very LR faces.

Recently, deep learning based face SR methods have been actively explored and achieved superior performance compared to traditional methods. Yu *et al.* [31], [32] develop GAN-based models to hallucinate very LR face images. Huang *et al.* [33] incorporate the wavelet coefficients into deep convolutional networks to super-resolve LR inputs with multiple upscaling factors. Cao *et al.* [9] design an attention-aware mechanism and a local enhancement network to alternately enhance facial regions in super-resolution. Xu *et al.* [34] jointly super-resolve and deblur face and text images with a multi-class adversarial loss. Dahl *et al.* [35] present an autoregressive Pixel-RNN [36] to hallucinate pre-aligned LR faces. Yu *et al.* [18] present a multiscale transformative discriminative network to hallucinate unaligned input LR face images with different resolutions. Zhang *et al.* [37] develop a two-branch super-resolution network to compensate and upsample ill-illuminated LR face images. However, these methods focus on super-resolving near-frontal LR faces. Thus, they are restricted to the inputs under small pose variations.

Several face SR techniques have been proposed to super-resolve LR faces under large pose variations by introducing facial prior information [4], [10], [38]. Chen *et al.* [10] incorporate facial geometry priors into their SR model to super-resolve LR faces. Yu *et al.* [4] exploit the facial component information from the intermediate upsampled features to encourage the upsampling stream to produce photo-realistic HR faces. However, these techniques only super-resolve non-frontal LR faces without frontalizing them for better visual perception.

B. Face Frontalization

Frontal view synthesis, termed as face frontalization, is a challenging task for its ill-posed nature, such as self-occlusions and pose variations. Conventional and emerging researches on face frontalization can be grouped into three classes: 2D/3D local feature warping, statistic modeling as well as deep learning based methods.

The first category researches date back to the 3D Morphable Model (3DMM) [16], which extracts the shape and texture bases of a face in PCA subspace. Driven by 3DMM, Yang *et al.* [39] formulate new expressions of input faces

by estimating 3D surface from face appearance. Meanwhile, approaches [17], [40], [41], [41]–[44] generate frontal faces by mapping a non-frontal face onto a 3D reference surface mesh. However, detecting facial landmarks [45] is the fundamental prerequisite for these approaches to determine the transformation between the query image and template. Thus, they fail to address the face images with extreme yaw angles or in low resolutions.

Considering that frontal faces has the minimum rank of all various poses, another face frontalization research stream focuses on inferring frontal views by solving a low-rank constrained minimization problem of statistical models. Sagonas *et al.* [13] achieve joint face frontalization and facial landmark detection in a whole framework. However, their results cannot ensure that the frontalized faces are consistent with the ground-truth frontal ones.

More recently, deep learning based methods [5], [12], [15], [46]–[50] have been leveraged for face frontalization research. Kan *et al.* [51] design stacked auto-encoders to progressive frontalize non-frontal HR faces based on the learned pose-robust features. Cole *et al.* [48] present a face recognition network to decompose an input face image into facial landmarks and aligned texture maps. Then, a differentiable image warping operation is conducted to produce the frontal view. Tuan *et al.* [52] propose a CNN-based model to learn 3DMM shapes as well as texture parameters. However, they render frontal faces without taking the image intensity similarity into consideration, resulting in distorted results.

Later, image generative models [53] have been widely employed for face frontalization. Tran *et al.* [5] propose a GAN-based model to learn the disentangled representation of input faces, achieving label-assisted face frontalization and pose-invariant face recognition. Jie *et al.* [54] propose a high fidelity pose invariant model to synthesize frontal faces from estimated dense correspondence fields and recovered facial texture maps.

Above all, face frontalization is treated as an HR image-to-image translation problem without taking face SR into consideration simultaneously. On the contrary, our goal is to frontalize profile faces in low resolution as well as super-resolve facial details at the same time.

III. PROPOSED METHOD: VIVIDGAN

Our VividGAN consists of a Vivid-FHnet that comprises a coarse-level FH network and a fine-level FH network, and two discriminators, *i.e.*, Coarse-D and Fine-D. We let the coarse-level FH network provide a preview for the fine-level FH network. Meanwhile, two-level discriminators are introduced to force the hallucinated frontal HR faces to be authentic as real frontal face images.

A. Coarse-level FH Network

Our coarse-level FH network is designed to recover a frontal coarse HR face image. The architecture of our coarse-level FH network is illustrated in Fig. 3. An input LR face is firstly encoded to latent features. Then, we hallucinate the latent features by a cascade of Feature Transform modules (FT

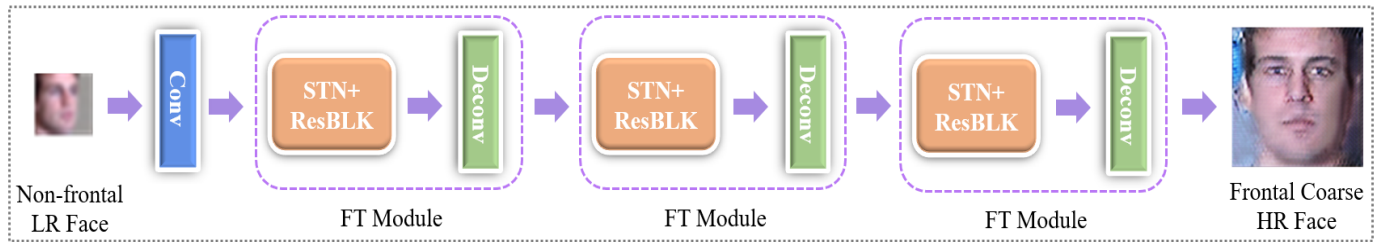


Fig. 3: The architecture of our coarse-level FH network.

module) composed of a spatial transform network (STN) [6], a residual block [55], and a deconvolutional layer. Inspired by [7], [18], in each FT module, the spatial transform network (STN) [6] layer is used to line up the intermediate features. Afterwards, the deconvolutional layer is adopted to upsample the aligned features. Meanwhile, the residual block [55] is introduced to improve the recovery of high-frequency details and the network capacity. Since the STN and upsampling layers are interwoven together, our coarse-level FH network can effectively eliminate misalignments.

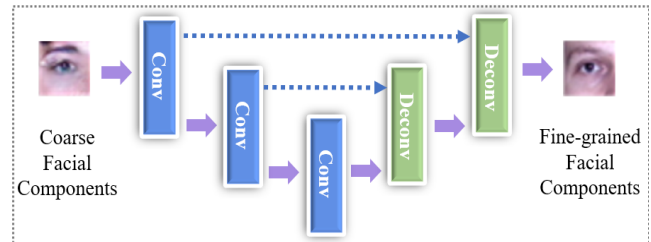
To minimize discrepancies between output images and ground-truth images, our network is trained using two losses: the first one is a pixel-wise l_2 loss to maintain the pixel-wise intensity similarity and the second one is a perceptual loss [56] to enforce the feature-wise high-level similarity. To cope with the self-occlusion and preserve the content-integrity in output images, we introduce a mirror symmetry loss. To enforce the output images to resemble real ones, a discriminative loss is also employed. As shown in Fig. 6(b), our coarse-level FH network effectively performs face SR and frontalization on the unaligned non-frontal LR face, which provides a more precise facial skeleton for subsequent touch-ups.

B. Fine-level FH Network

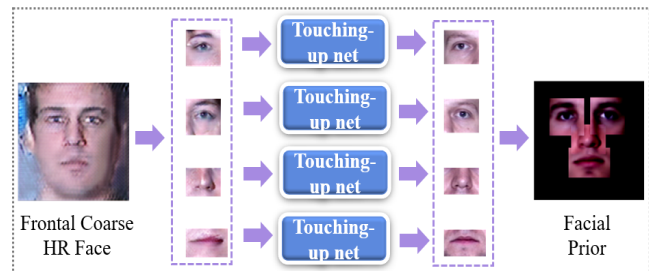
Our fine-level FH network is proposed to recover facial fine details of HR frontal faces by explicitly exploiting the facial component appearance prior, *i.e.*, detailed facial components. First, we design a touching-up subnetwork to recover the fine details of each facial component. The recovered facial components will be exploited as priors to recover high-quality frontal face images. Then, we develop a fine-integration subnetwork to merge the frontal coarse HR face and the facial component appearance prior in a seamless fashion.

1) *Touching-up subnetwork*: After obtaining the frontal coarse HR face, obscure details of the vital facial components, *i.e.*, eyes, noses, mouths, become more distinguishable and can be easily cropped out based on detected facial landmarks now. Here, the landmark localization can be obtained by a widely-used facial landmark detector [57]. With the cropped parts, we design a touching-up subnetwork to refine the coarsely upsampled facial components and estimate the fine details for each component (see Fig. 4(a)).

Inspired by the U-net architecture [58], our touching-up subnetwork employs successive convolutional and deconvolutional layers along with skip connections to enhance features of each component. In this way, multi-scale features of facial components can be integrated to achieve photo-realistic results.



(a) The architecture of the touching-up subnetwork



(b) The generation procedure of the facial component appearance prior

Fig. 4: The detail of our touching-up subnetwork.

Towards this goal, we establish facial component sets of the regions of left eyes, right eyes, noses and mouths on the Multi-PIE database [59], the MMI Facial Expression (MMI) database [60], the Celebrity Face Attribute (CelebA) database [61] and our proposed PSD-HIGHROAD database [62], respectively, which covers the traits from different genders, races, ages and facial expressions.

We pre-train the touching-up subnetwork with a pixel-wise intensity similarity loss on these facial component sets for parameter initialization. Afterwards, the estimated fine-grained facial components are stitched onto a masked template as our facial component appearance prior (see Fig. 4(b)). Meanwhile, the max-out fusing strategy is adopted to reduce the stitching artifacts on the overlapping areas.

2) *Fine-integration subnetwork*: We feed the facial component appearance prior and the frontal coarse HR face as a blueprint into a fine-integration subnetwork for further refinement. Our fine-integration subnetwork generates the frontal fine HR face in three steps, as illustrated in Fig. 5(a): (i) an *encoder* concatenates the frontal coarse HR face and the component appearance prior to produce the fused features, denoted as F_C ; (ii) a *facial component-aware module* aligns and merges the coarsely restored face and the stitched facial components in the feature level; (iii) a *decoder* reconstructs a frontal fine HR face. In the fine-integration subnetwork, the encoder and decoder adopt the same architectures as

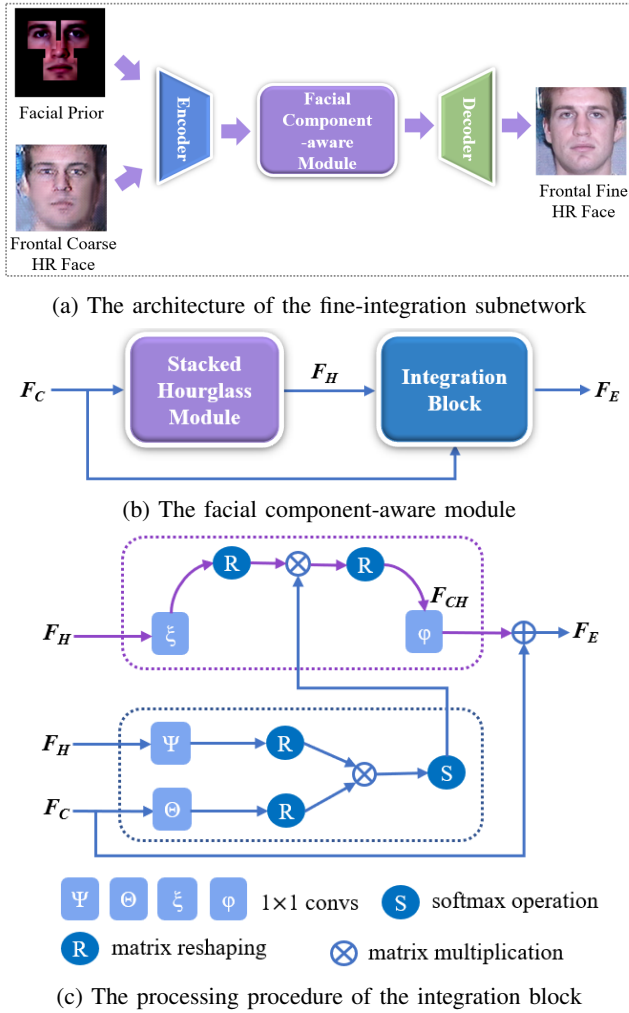


Fig. 5: The detail of our fine-integration subnetwork.

our coarse-level FH network except that the encoder of the fine-integration subnetwork takes two images as input (*i.e.*, a coarsely frontalized and upsampled face and a stitched component prior image).

Our newly designed facial component-aware module consists of a stacked hourglass network [63] and an integration block (see Fig. 5(b)). First, we introduce a stacked hourglass network [63] to estimate the facial landmark heatmaps from the fused features. Then, we feed the facial landmark heatmaps and the fused features to an integration block for re-calibration.

Fig. 5(c) illustrates the re-calibration procedure in our integration block. The facial landmark heatmaps F_H and the fused features F_C are first normalized and transformed into two feature spaces θ and ψ to measure their similarity. Then, the attended features F_{CH} are formulated as a weighted sum of the facial landmark heatmaps F_H that are similar to the fused features F_C in the corresponding positions. The i -th output response is expressed as:

$$F_{CH}^i = \frac{1}{M(F)} \sum_{\forall j} \left\{ \exp \left(W_{\theta}^T \left(\overline{F_C}^i \right)^T \overline{F_H^j} W_{\psi} \right) F_H^j W_{\zeta} \right\}, \quad (1)$$

where $M(F) = \sum_{\forall j} \exp \left(W_{\theta}^T \left(\overline{F_C}^i \right)^T \overline{F_H^j} W_{\psi} \right)$ is the sum of all output responses over all positions. In Eq. (1), the embedding

transformations W_{θ} , W_{ψ} and W_{ζ} are learnt in training.

Finally, we integrate the fused features F_C and the attended features F_{CH} to form the final refined features F_E , as follows:

$$F_E = \sigma \left(F_{CH} W_{\phi} \right) + F_C, \quad (2)$$

where W_{ϕ} is also learnt during the training process. σ is a trade-off parameter, and is set to 1 in our experiment. As a result, our integration block provides spatial configuration of facial components.

During training, we employ a pixel-wise intensity similarity loss, a feature-wise identity similarity loss [56], a structure-wise similarity loss [19] and a discriminative loss. Once our fine-integration subnetwork is trained, it is able to achieve frontal HR faces with authentic facial details (see Fig. 6(j)).

To verify the effectiveness of our facial component-aware module, we conduct some comparisons. As shown in Fig. 6(f), the VividGAN variant without the facial component-aware module produces inferior results. On the contrary, our facial component-aware module achieves superior feature alignment and enhancement.

C. Two-level Discriminators

Our Vivid-FHnet hallucinates non-frontal LR faces in a coarse-to-fine manner and produces high-quality HR faces. Inspired by [18], [19], we employ a discriminative network to force the generated faces to lie on the same manifold as real frontal faces. However, a single discriminator commonly used in previous works [7], [18], [19], [32], [64] might not be suitable for our two-level face hallucination. Thus, we propose two-level discriminators, *i.e.*, Coarse-D and Fine-D, to address these two types of recovered HR faces. The Coarse-D enforces a coarsely hallucinated face to be an upright and complete preview; while the Fine-D focuses on the fine hallucinated one for more sharper details.

To analyse the effect of our two-level discriminators, we perform different VividGAN variants, as shown in Figs. 6(g),(h),(i) and (j). It can be obviously seen that our VividGAN (Fig. 6(j)) captures both the global outline of the face as well as detailed facial characteristics.

D. Objective Functions

In our work, we employ five individual losses to train our networks, including a mirror symmetry loss (L_{sys}), a pixel-wise intensity similarity loss (L_{mse}), a feature-wise identity similarity loss (L_{id}), a structure-wise similarity loss (L_h) and a class-wise discriminative loss (L_{adv}).

1) *Mirror symmetry loss*: Human faces, like many biological forms, manifest high degrees of symmetry. Thus, we introduce a mirror symmetry loss (L_{sys}) to guarantee the content integrity of hallucinated faces. The mirror symmetry loss L_{sys} of a generated image \hat{h}_i is formulated as:

$$L_{sym} = \mathbb{E}_{(\hat{h}_i) \sim p(\hat{h})} \left\| \vec{h}_i - \vec{h}_i^T \right\|_F^2, \quad (3)$$

where \vec{h}_i represents the horizontally flipped copy of a generated face \hat{h}_i .

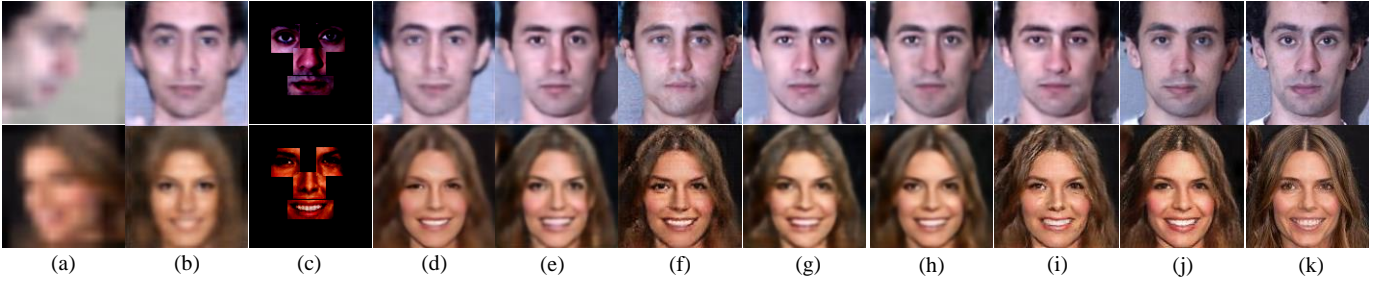


Fig. 6: Ablation study on the effect of different sub-nets and losses on Multi-PIE and CelebA databases. (a) The input non-frontal LR images (16×16 pixels). (b) The frontal coarse HR faces. (c) The fine-grained facial components. (d) The results only using L_{mse} and L_h . (e) The results using L_{mse} , L_{id} and L_h . (f) The results of VividGAN w/o facial component-aware module (w/o L_h). (g) The results of Vivid-FHnet. (h) The results of Vivid-FHnet and Coarse-D. (i) The results of Vivid-FHnet and Fine-D. (j) The results of VividGAN. (k) The ground-truth frontal HR images (128×128 pixels).

2) *Pixel-wise intensity similarity loss*: In order to force the hallucinated face to be close to its ground-truth, an intensity similarity loss L_{mse} is employed, defined as:

$$L_{mse} = \mathbb{E}_{(\hat{h}_i, h_i) \sim p(\hat{h}, h)} \|\hat{h}_i - h_i\|_F^2, \quad (4)$$

where $p(\hat{h}, h)$ represents the joint distribution of the generated results \hat{h}_i and the corresponding ground-truths h_i .

As mention in [65], only employing pixel-wise intensity similarity losses L_{mse} in training often leads to overly smoothed results and the network may fail to generate high-frequency facial features (see Fig. 6(d)). Therefore, we incorporate a feature-wise identity similarity loss to enhance our hallucinated results.

3) *Feature-wise identity similarity loss*: Identity preservation is one of the most important goals in face hallucination [66]. Thus, we adopt the identity similarity loss L_{id} by measuring the Euclidean distance between the high-level features of a hallucinated face and its ground-truth, thus endowing our VividGAN with the identity preserving ability. The identity similarity loss L_{id} is expressed as:

$$L_{id} = \mathbb{E}_{(\hat{h}_i, h_i) \sim p(\hat{h}, h)} \|\Phi(\hat{h}_i) - \Phi(h_i)\|_F^2, \quad (5)$$

where $\Phi(\cdot)$ represents the extracted feature vector from the average pooling layer of the Resnet50 model [55] for the input images. As seen in Fig. 6(e), employing L_{id} indeed improves the generated results while producing more authentic facial details.

4) *Structure-wise similarity loss*: To localize spatial configuration of facial components, a structure-wise similarity loss [19] L_h is employed in training our facial component-aware module, written as:

$$L_h = \mathbb{E}_{(l_i, h_i) \sim p(l, h)} \frac{1}{P} \sum_{k=1}^P \left\| H^k(f_i) - H^k(h_i) \right\|_2^2, \quad (6)$$

where $H^k(f_i)$ represents the k -th predicted facial landmark heatmap estimated from the intermediate facial features f_i by a stacked hourglass module. $H^k(h_i)$ denotes the k -th facial landmark heatmap generated by FAN [67] on the ground-truth image h_i . Here, we use 68 point facial landmarks to produce a heatmap.

5) *Class-wise discriminative loss*: Aiming at generating photo-realistic results, we infuse the class discriminative information into our Vivid-FHnet by adopting the two-level discriminators. Our goal is to let the two-level discriminators fail to distinguish hallucinated faces from ground-truth ones. The objective function L_D for the discriminator is defined as follows:

$$L_D = -\mathbb{E}_{(\hat{h}_i, h_i) \sim p(\hat{h}, h)} [\log D_d(h_i) + \log(1 - D_d(\hat{h}_i))], \quad (7)$$

where D and d represent the discriminator and its parameters. During training, we minimize the loss L_D and update the parameters for the discriminator.

On the contrary, our Vivid-FHnet is designed to produce realistic face images, which would be classified as real faces by the discriminators. Thus, the discriminative loss L_{adv} is represented as:

$$L_{adv} = -\mathbb{E}_{\hat{h}_i \sim p(\hat{h})} \log(D_d(\hat{h}_i)). \quad (8)$$

To optimize the Vivid-FHnet, we minimize the loss L_{adv} .

E. Training Details

Since different subnetworks focus on different goals, we use different losses to train our coarse-level FH network, touching-up subnetwork and fine-integration subnetwork.

The objective function for the coarse-level FH network, L_C , is expressed as:

$$L_C = L_{mse}^c + L_{sys}^c + \alpha_1 L_{id}^c + \psi_1 L_{adv}^c. \quad (9)$$

The objective function for the touching-up subnetwork, L_T , is expressed as:

$$L_T = L_{mse}^t. \quad (10)$$

The objective function for the fine-integration subnetwork, L_F , is expressed as:

$$L_F = L_{mse}^f + \alpha_2 L_{id}^f + \gamma_2 L_h^f + \psi_2 L_{adv}^f. \quad (11)$$

Above all, the total objective function for our Vivid-FHnet, L_G , is expressed as:

$$L_G = L_C + L_T + L_F. \quad (12)$$

Since we intend to hallucinate frontal HR faces to be close to ground-truth appearance, we set lower weights on L_{id} , L_h and L_{adv} . Thus, $\alpha_1, \psi_1, \alpha_2, \gamma_2$ and ψ_2 in Eq. (9), (10) and



Fig. 7: Illustration of facial components. The coarse facial components are shown in the first column, the fine-grained facial components are illustrated in the second column, and the ground-truth facial components are presented in the third column.

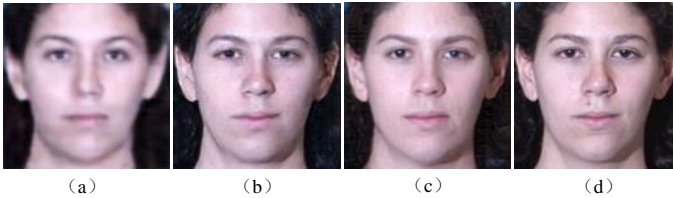


Fig. 8: Impacts of the facial component appearance prior. (a) Result of V-TN model (25.784/0.870 in PSNR/SSIM). (b) Result of VividGAN model (26.289/0.876 in PSNR/SSIM). (c) Result of V+GT model (**28.405/0.902** in PSNR/SSIM). (d) The ground-truth image.

(11) are set to 0.01. Moreover, the training process of our VividGAN model involves in three stages: (i) Pre-training the coarse-level FH network with loss L_C (Eq. (9)) on the training dataset for parameter initialization; (ii) Pre-training the touching-up subnetwork with loss L_T (Eq. (10)) on the facial component set for parameter initialization; (iii) Training the whole VividGAN model with three losses together: Vivid-FHnet is trained by L_G (Eq. (12)) and loss L_D (Eq. 7) is used to optimize Coarse-D and Fine-D. In the final stage, since our fine-integration subnetwork has not been initialized, the learning rate for training our fine-integration subnetwork is set to 10^{-3} while the learning rate for training the other networks is set to 10^{-4} .

IV. PRIOR KNOWLEDGE FOR JOINT FACE SR AND FRONTALIZATION

Most of real-world objects have their distinct structured appearances, like human faces. In this paper, we model and leverage the facial component appearance prior to facilitate joint face SR and frontalization. As a consequence, there are two questions worthy of exploring: (i) Is the facial component appearance prior knowledge useful for joint face SR and frontalization? (ii) How many improvements will it bring?

To answer the above questions, we conduct subjective and objective experiments on the Multi-PIE database [59]. Multi-PIE provides non-frontal/frontal face pairs of 337 individuals under various poses and illumination conditions. We introduce 45K face pairs, consisting of non-frontal faces ($\pm 15^\circ$, $\pm 30^\circ$, $\pm 45^\circ$, $\pm 60^\circ$, $\pm 75^\circ$, $\pm 90^\circ$) and corresponding frontal faces (0°), to construct the training set. The rest 5K face pairs are used for testing.

A. Baseline Models

We formulate two baseline models to verify that the facial component appearance prior knowledge is important for joint face SR and frontalization.

The baseline models are summarized as follows (Here, we denote VividGAN as V, touching-up network as TN, and ground-truth as GT):

- V-TN: we remove the touching-up subnetwork, and construct the “V-TN” model. “V-TN” model consists of the coarse-level FH network and the fine-integration subnetwork.
- V+GT: we introduce the ground-truth facial component appearance prior, *i.e.*, ground-truth facial components, to replace the estimated prior of the touching-up subnetwork, constructing the “V+GT” model.

B. Importance of Facial Component Prior

The results of the compared models are illustrated in Fig. 8. As we can see, the results in Figs. 8(b) and (c) show more vivid facial details than the result in Fig. 8(a). This clearly manifests the importance of the facial prior knowledge in the hallucination process. As indicated in Fig. 8, V+GT model (with the ground-truth facial component appearance prior) outperforms VividGAN model (with the estimated facial component appearance prior) and V-TN model (without prior information) with the PSNR improvement of 2.116 dB and 2.621 dB, respectively. Therefore, our VividGAN provides a solution to hallucinating better fine-grained facial components, as shown in Fig. 7, and significantly improve the visual quality of the hallucinated faces.

V. EXPERIMENTS

A. Experimental Setup

1) *Databases*: VividGAN is trained and tested on multiple widely used benchmarks, *i.e.*, the Multi-PIE database [59], the MMI facial expression database [60] and the CelebA database [61].

Multi-PIE [59] has been described in Sec. IV. **CelebA** [61] is a large in-the-wild database that contains more than 200,000 face images under different pose, occlusion and background variations. **MMI** [60] contains 2,900 videos and HR still images of 75 individuals. We extract the frames of the individuals



Fig. 9: Illustration of the synthesized non-frontal faces. First line: the synthesized non-frontal LR faces; second line: the corresponding HR ones.

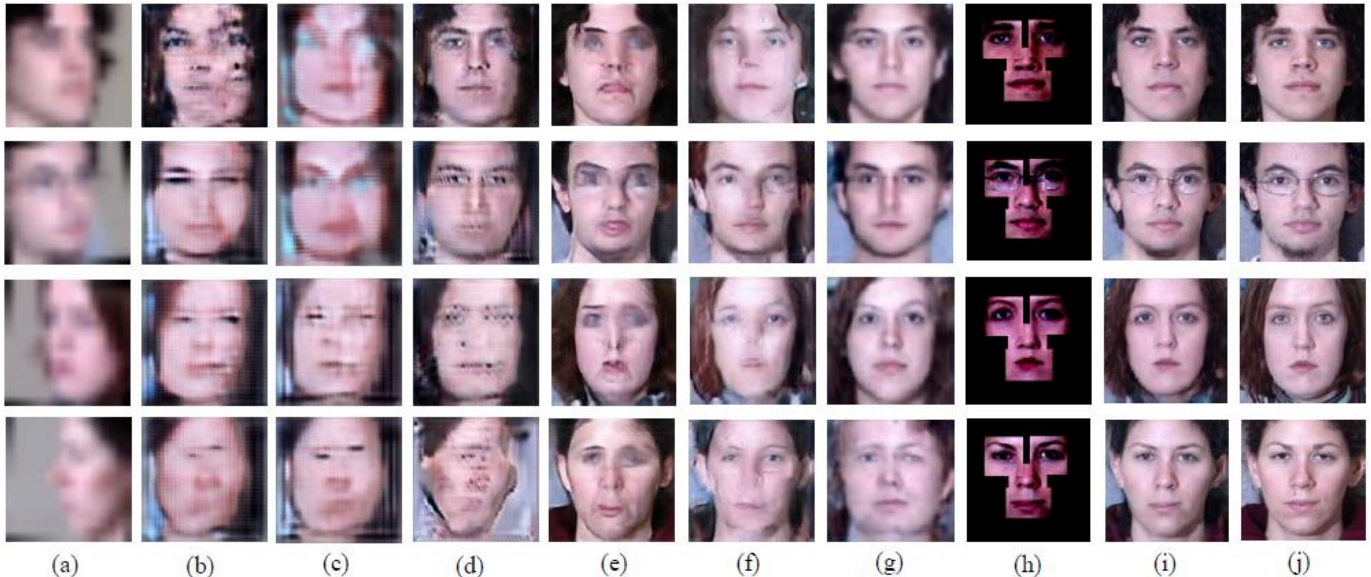


Fig. 10: Qualitative comparisons of state-of-the-art methods on the Multi-PIE database. Columns: (a) Unaligned LR inputs under various poses (Rows: $+60^\circ$, $+45^\circ$, -75° and -90°). (b) Bicubic + [5] (c) [5] + [8]. (d) [5] + [33]. (e) [65] + [5]. (f) [32] + [5]. (g) [7]. (h) Fine-grained facial components. (i) VividGAN. (j) Ground-truths.

from their facial expression sequences. Each of these frames is labeled as one of seven basic expressions, *i.e.*, “angry”, “disgust”, “fear”, “happy”, “sad”, “surprise”, and “neutral”.

On the **Multi-PIE** database, we employ 50K face pairs consisting of non-frontal faces ($\pm 15^\circ$, $\pm 30^\circ$, $\pm 45^\circ$, $\pm 60^\circ$, $\pm 75^\circ$, $\pm 90^\circ$) and corresponding frontal faces (0°), for experiments. **CelebA** and **MMI** databases do not provide frontal/non-frontal face pairs. Thus, following [7], we use a popular 3D face model [44] to synthesize non-frontal HR face images, *i.e.*, $\{\pm 22^\circ, \pm 40^\circ, \pm 55^\circ, \pm 75^\circ\}$, from frontal HR ones for training. Here, we first randomly select 10,000 and 900 cropped frontal HR faces from CelebA and MMI databases, resize them to 128×128 pixels, and use them as our ground-truth images. Then, we generate the unaligned non-frontal LR faces (16×16 pixels) by transforming and downsampling the synthesized non-frontal HR ones. Fig. 9 illustrates some synthesized non-frontal faces. In this manner, we generate 80,000 and 7,200 unaligned non-frontal LR/frontal HR face pairs for CelebA and MMI databases. Finally, for each database, we choose 80 percent of the face pairs for training and 20 percent of the face pairs for testing, respectively. In this way, the training and testing sets do not overlap.

2) *Competing methods*: We conduct comparative experiments in the following three fashions:

- **F+SR**: face frontalization techniques (DRGAN [5] or Hassner *et al.* [14]) followed by face SR methods (SRGAN [65], CBN [8], WaveletSRnet [33] or TDAE [32]) (we use bicubic interpolation to adjust image sizes);
- **SR+F**: face SR methods (SRGAN [65], CBN [8], WaveletSRnet [33] or TDAE [32]) followed by face frontalization techniques (DRGAN [5] or Hassner *et al.* [14]);
- **Joint SR+F**: TANN [7] and our VividGAN.

In the first fashion (F+SR), we first frontalize the non-frontal LR faces by popular frontalization techniques, and then super-resolve the frontalized faces by state-of-the-art SR methods. In the second fashion (SR+F), we first super-resolve the non-frontal LR faces, and then frontalize the upsampled results. In the third fashion (Joint SR+F), both TANN [7] and VividGAN jointly tackle face SR and face frontalization in a unified framework.

For a fair comparison, we retrain these baseline methods on our training sets. Since SRGAN [65], CBN [8] and WaveletSRnet [33] cannot achieve face alignment during their upsampling procedure, we train a STN [6] to align the input unaligned LR faces to the upright position firstly. However, TANN [7], TDAE [32] and our VividGAN do not need any

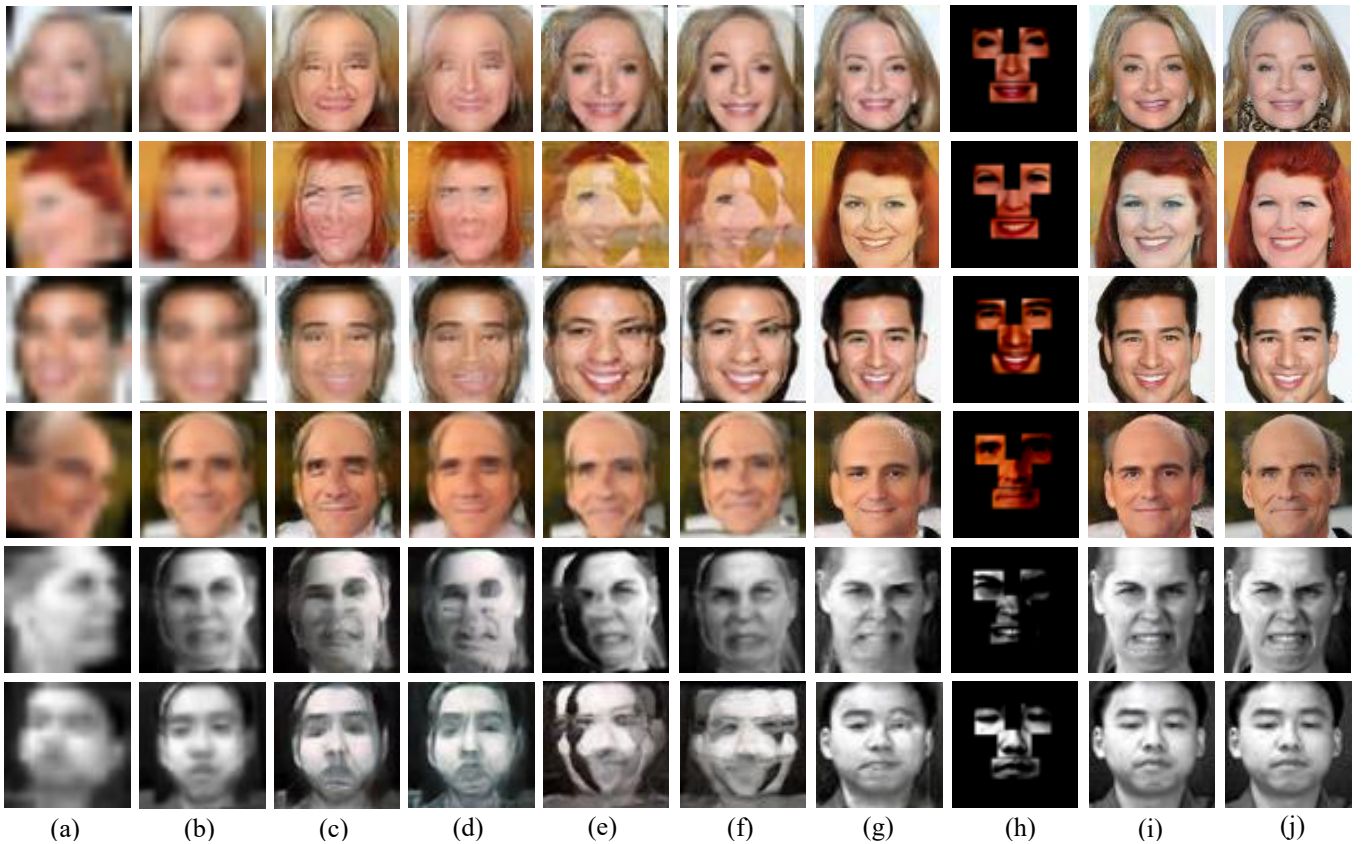


Fig. 11: Qualitative comparisons of state-of-the-art methods on CelebA and MMI databases. Columns: (a) Unaligned LR inputs under various poses (Rows: -40° , -75° , -22° , $+75^\circ$, $+75^\circ$ and -40°). (b) Bicubic + [14]. (c) [14] + [8]. (d) [14] + [33]. (e) [65] + [14]. (f) [32] + [14]. (g) [7]. (h) Fine-grained facial components. (i) VividGAN. (j) Ground-truths.

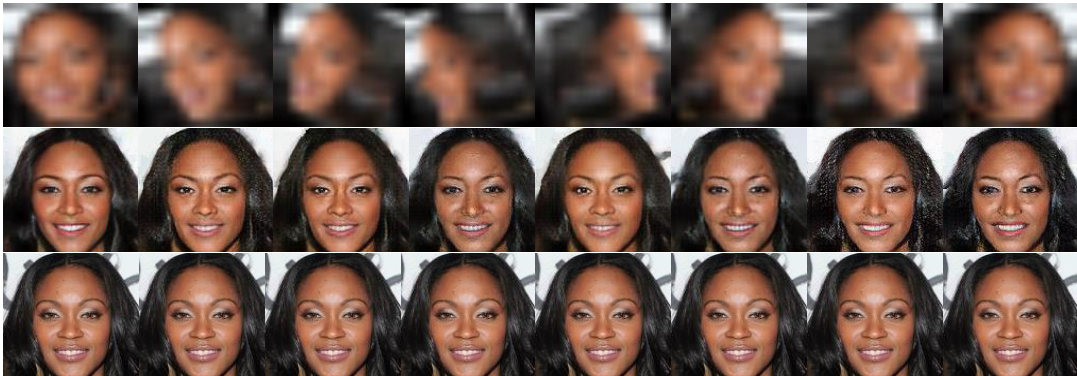


Fig. 12: Results of our VividGAN. First row: the input unaligned LR faces under various poses; second row: our hallucinated results; third row: the ground-truth frontal HR face images.

alignment in advance and generate upright results automatically. Furthermore, compared to DRGAN [5] and Hassner *et al.* [14], our VividGAN does not need auxiliary poses or facial landmarks for face frontalization.

B. Qualitative Evaluation

Figs. 10 and 11 illustrate the visual results of the compared methods. The hallucinated results obtained by VividGAN are more photo-realistic and identity-preserving.

As shown in Figs. 10(b) and 11(b), the combination of bicubic interpolation and frontalization methods [5], [14] fails

to generate photo-realistic facial details. Since bicubic upsampling only interpolates new pixels from neighboring pixels without generating new contents, the produced non-frontal HR images lack details. Thus, the face frontalization method fails to detect facial landmarks and outputs erroneous frontalized faces with severe artifacts and distorted contours.

As discussed in Sec. I, simply combining existing face SR and frontalization methods cannot address this challenging issue. This is verified by the results of the F+SR methods (see Figs. 10(c), 10(d), 11(c) and 11(d)), where upsampled face regions suffer severe distortions and ghosting artifacts. Similarly, the SR+F methods also fail to recover authentic

TABLE I: Average PSNR [dB] and SSIM values of the competing methods on the entire testing sets.

SR Method	Multi-PIE		MMI		CelebA		Multi-PIE		MMI		CelebA	
	F [5]+SR						SR+F [5]					
	PSNR	SSIM										
Bicubic	21.352	0.803	21.670	0.812	21.055	0.802	18.991	0.730	19.125	0.738	20.956	0.799
SRGAN [65]	21.562	0.804	21.328	0.809	20.996	0.800	19.235	0.733	19.958	0.744	20.072	0.794
CBN [8]	21.974	0.806	20.846	0.792	20.073	0.794	20.251	0.752	20.006	0.749	19.784	0.783
WaveletSRnet [33]	22.839	0.811	22.005	0.817	21.831	0.817	21.164	0.798	20.752	0.762	21.079	0.805
TDAE [32]	22.649	0.824	22.124	0.819	20.708	0.796	20.032	0.749	20.353	0.753	20.353	0.796
TANN [7]	24.426	0.831	23.748	0.845	25.690	0.870	24.426	0.831	23.748	0.845	25.690	0.870
VividGAN [†]	21.078	0.805	21.264	0.810	22.181	0.832	21.078	0.805	21.264	0.810	22.181	0.832
VividGAN	26.289	0.876	26.452	0.881	26.965	0.893	26.289	0.876	26.452	0.881	26.965	0.893

VividGAN[†] represents the coarse-level FH network in VividGAN.

TABLE II: Quantitative evaluations on different out-of-plane rotation degrees on CelebA and MMI testing sets.

SR Method	$\pm 22^\circ$		$\pm 40^\circ$		$\pm 55^\circ$		$\pm 75^\circ$	
	CelebA	MMI	CelebA	MMI	CelebA	MMI	CelebA	MMI
	F [5] +SR							
Bicubic	21.648/0.817	22.341/0.800	21.167/0.815	21.976/0.788	20.004/0.798	19.678/0.761	18.982/0.791	18.904/0.749
SRGAN [65]	21.877/0.819	22.109/0.797	21.032/0.814	21.893/0.787	18.989/0.790	19.241/0.752	17.335/0.758	18.036/0.741
CBN [8]	21.004/0.814	22.843/0.806	20.838/0.810	22.132/0.798	19.104/0.793	18.947/0.749	17.893/0.780	17.405/0.733
WaveletSRnet [33]	22.951/0.829	24.005/0.826	22.004/0.822	23.346/0.817	20.752/0.808	19.901/0.762	19.004/0.792	18.536/0.747
TDAE [32]	21.728/0.818	22.903/0.810	21.003/0.814	22.142/0.798	19.652/0.794	19.096/0.751	18.126/0.785	18.002/0.740
SR+ F [5]								
Bicubic	21.049/0.816	20.052/0.749	21.040/0.815	19.233/0.729	19.901/0.795	17.036/0.703	17.452/0.760	16.021/0.683
SRGAN [65]	21.080/0.816	20.991/0.764	20.562/0.809	20.148/0.750	19.073/0.790	18.200/0.718	17.066/0.756	17.005/0.700
CBN [8]	20.683/0.802	20.984/0.763	19.991/0.806	20.571/0.761	18.392/0.787	18.852/0.731	16.183/0.702	17.003/0.699
WaveletSRnet [33]	22.004/0.822	22.341/0.798	21.358/0.818	21.860/0.772	19.996/0.796	18.741/0.729	17.742/0.764	16.975/0.692
TDAE [32]	21.758/0.819	21.042/0.767	21.041/0.815	20.248/0.752	19.425/0.792	18.015/0.716	17.002/0.755	16.897/0.690
Joint SR+F								
TANN [7]	26.709/0.882	24.923/0.866	25.910/0.874	24.052/0.852	25.362/0.870	23.104/0.841	24.975/0.868	22.621/0.834
VividGAN	28.254/0.902	27.490/0.893	27.792/0.898	26.601/0.884	26.667/0.889	25.712/0.876	26.105/0.882	25.039/0.869

In each cell, the first and second numbers denote PSNR [dB] and SSIM values, respectively.

facial details (see Figs. 10(e), 10(f), 11(e) and 11(f)).

TANN [7] is the first attempt to jointly address face SR and face frontalization in a whole framework. In this manner, two tasks alternately facilitate each other. Thus, TANN generates satisfying results, as shown in Figs. 10(g) and 11(g). However, due to its single-stage mechanism, TANN does not have a “looking back” mechanism to revise the hallucinated faces. Therefore, when input LR faces undergo extreme poses (see the forth row in Fig. 10(a)) or complex expressions (see the fifth and sixth rows in Fig. 11(a)), TANN produces distorted facial details. Moreover, the hallucinated faces suffer mild blurs, as visible in Fig. 10(g) and Fig. 11(g).

Our VividGAN generates photo-realistic frontal HR faces from very LR inputs with various poses and expressions in Figs. 10(i), 11(i) and 12. Moreover, VividGAN is able to revise facial details and thus obtains visually appealing HR face images (*e.g.*, the mouth in the fifth row of Fig. 11(i) and the “slight closed eyes” in the sixth row of Fig. 11(i)). Since our VividGAN hallucinates non-frontal LR faces in a coarse-to-fine manner and embodies a revision mechanism, it reconstructs fine facial details and achieves superior hallucination performance.

C. Quantitative Evaluation

Following the quantitative evaluation in TANN, we also report average PSNR and SSIM values on the testing sets in two different manners (see Tabs. I and II).

TABLE III: Ablation study of different losses

	Multi-PIE		CelebA	
	PSNR	SSIM	PSNR	SSIM
L_G^-	23.017	0.779	22.945	0.773
L_G^+	24.332	0.803	23.981	0.798
L_G^\pm	25.998	0.845	25.057	0.804
L_G^*	26.055	0.874	26.128	0.885
L_G	26.289	0.876	26.965	0.893

As shown in Tab. I, our VividGAN achieves remarkable quantitative results than other state-of-the-art methods on both under-controlled and in-the-wild databases. Specifically, on the MMI testing set, VividGAN outperforms the second best technique TANN with a large margin of approximate 2.7 dB in PSNR. This is mainly due to our fine-level FH network that not only exploits facial component priors but also processes a revision mechanism. Thus, the hallucinated faces by our VividGAN are more similar to the ground-truths.

As presented in Tab. II, VividGAN achieves the best performance across all poses, especially for large yaw angles. Moreover, as the rotation angle increases, our method does not degrade like the other methods. In the extremely challenging angles ($\pm 75^\circ$), VividGAN outperforms the second best TANN more than 1 dB in PSNR. This also verifies that VividGAN attains more authentic results when the input LR faces are under extreme poses.

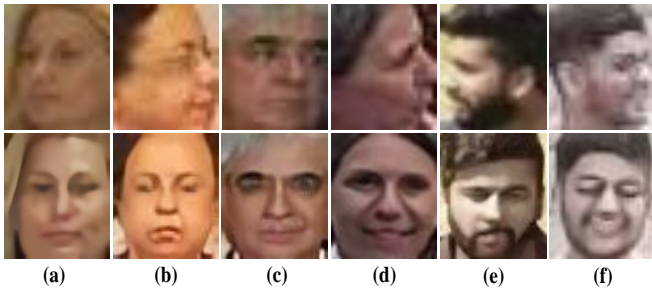


Fig. 13: Results on LR face images in the wild. Top row: LR images in the wild. Bottom row: our hallucinated results.

TABLE IV: Efficiency comparison on the CelebA testing set.

Method		Parameter Number (KB)	Running Time (ms)	PSNR (dB)
F+SR/ SR+F	SRGAN [65]	278,758	30.41	20.072/20.996
	CBN [8]	270,562	2028.23	19.784/20.073
	WaveletSRnet [33]	324,458	31.68	21.097/21.831
	TDAE [32]	286,293	50.42	20.353/20.708
Joint SR+F	TANN [7]	196,231	15.60	25.690
	VividGAN [†]	103,473	13.12	22.181
	VividGAN	242,089	19.25	26.965

VividGAN[†] represents the coarse-level FH network in VividGAN.

D. Ablation Analysis

We report the performance of different VividGAN variants, which are trained with different loss combinations, on Multi-PIE and CelebA (see Tab. III and Fig. 6). We denote the compared VividGAN variants as follows: (i) $L_G^-: L_{mse}, L_h$; (ii) $L_G^{\dagger}: L_{mse}, L_{id}$ and L_h ; (iii) $L_G^{\ddagger}: L_{mse}, L_{id}, L_h$ and L_{sys} ; (iv) $L_G^*: L_{mse}, L_{id}, L_h, L_{sys}$ and L_{adv}^c ; (v) $L_G: L_{mse}, L_{id}, L_h, L_{sys}, L_{adv}^c$ and L_{adv}^f . Note that L_h is a prerequisite constraint in training our facial component-aware module.

As demonstrated in Tab. III, only adopting intensity similarity loss L_{mse} leads to unpleasant quantitative results (L_G^- in Tab. III). The identity similarity loss L_{id} not only improves the visual quality (see Fig. 6(e)) but also increases the quantitative performance (L_G^{\dagger} in Tab. III). This experiment asserts that L_{id} forces the high-order moments of the hallucinated faces, *i.e.*, feature maps, to be similar to their ground-truths and thus improves hallucination performance. In addition, we also verify the effectiveness of the mirror symmetry loss L_{sys} . As indicated in Tab. III (L_G^{\ddagger}), using L_{sys} leads to better quantitative performance. Since L_{sys} enforces the content integrity of frontalized faces, it is able to reduce the reconstruction errors of coarsely frontal HR faces in the coarse-level FH network rather than spreading the errors through the entire Vivid-FHnet. Thus, the fine-level FH network can focus on learning mappings between coarse and fine HR facial patterns. Moreover, as demonstrated in Tab. III (L_{adv}^c) and Fig. 6(h), the Coarse-D improves the quantitative performance by forcing the coarsely hallucinated faces to be frontal and aligned. However, Fig. 6(h) shows that the hallucinated faces still suffer from mild blurriness. Finally, the help of the two-level discriminators, VividGAN achieves photo-realistic images (see Fig. 6(j)) and the best performance (L_G in Tab. III).

TABLE V: Data partition and statistics of the databases in our face recognition experiments.

Database	Whole Dataset		Testing Dataset		C/U
	Identities	Images	Gallery	Probe	
Multi-PIE [59]	337	157,617	50	5,000	C
MMI [60]	75	7,200	16	896	C
CelebA [61]	10,177	202,599	1,000	8,000	U
TinyFace [68]	5,139	169,403	157,871	3728	U
DroneSURF [69]	58	786,813	24	48,000	U
IJB-C [70]	3,531	148,800	19,593 templates		U

‘C’ means under-controlled, and ‘U’ means unconstrained.

E. Performance on in-the-wild Non-frontal LR Faces

To demonstrate that our method can be effectively generalized to in-the-wild non-frontal LR faces, we randomly select face images from real-world unconstrained databases (*e.g.*, TinyFace [68], DroneSURF [69]) for evaluation. The in-the-wild LR face images are, in general, much blurrier than our training samples. Here, we train the VividGAN model on the CelebA training set and our proposed facial component sets. As shown in Fig. 13, our VividGAN achieves pleasant frontalization and hallucination performance on such challenging images, demonstrating that it is not restricted to certain poses and under-controlled scenarios. Four reasons account for this phenomenon:

- 1) Our coarse-level FH network super-resolves and frontalizes the input non-frontal LR face roughly, which provides a more precise facial skeleton for subsequent touch-ups. On top of this face blueprint, our fine-level FH network is tailored-designed to recover fine details of frontal HR face image by explicitly incorporating the facial component appearance prior, *i.e.*, fine-grained facial components. These networks seamlessly work together to reduce the differences of 3D models and poses between the training and testing LR faces.
- 2) We have established the facial component sets (see Sec. III. B) of vital facial components from the in-the-wild database, which cover the statistics from a wide range of faces. Our touching-up subnetwork is fed with these facial component sets to provide an informative prior of vivid facial components. Thus, it can effectively hallucinate the fine-grained facial components in real-world scenarios.
- 3) Our proposed facial component-aware module leverages the facial landmark heatmaps as queries to accurately locate the corresponding vital facial parts. This module not only facilitates alignment but also provides spatial configuration of facial components, such as the shape of mouth. Thus, our method is able to produce visually pleasing HR facial details.
- 4) When generating our training set, the selected faces used for generating non-frontal faces are not required to be exactly frontal ones, which increases the variety of the training poses and thus provides flexibility to handle in-the-wild LR faces.

TABLE VI: Face recognition performance comparison on under-controlled and in-the-wild databases.

Database	Multi-PIE [59]				CelebA [61]				MMI [60]			
Settings	32 × 32, 4×		16 × 16, 8×		32 × 32, 4×		16 × 16, 8×		32 × 32, 4×		16 × 16, 8×	
Metric	Rank-1	Rank-5	Rank-1	Rank-5	Rank-1	Rank-5	Rank-1	Rank-5	Rank-1	Rank-5	Rank-1	Rank-5
LR face	51.08%	62.34%	40.26%	48.70%	3.85%	9.60%	1.75%	6.15%	11.28%	18.42%	8.71%	13.73%
TANN [7]	74.04%	80.32%	68.50%	73.16%	83.40%	89.55%	81.35%	86.70%	68.30%	79.13%	59.71%	67.97%
Vivid-GAN	85.36%	88.04%	82.28%	84.64%	87.60%	91.85%	84.20%	89.30%	79.13%	90.74%	70.20%	84.15%
Database	TinyFace [68]				DroneSURF [69]				IJB-C [70]			
Settings	32 × 32, 4×		16 × 16, 8×		32 × 32, 4×		16 × 16, 8×		32 × 32, 4×		16 × 16, 8×	
Metric	Rank-1	Rank-5	Rank-1	Rank-5	Rank-1	Rank-5	Rank-1	Rank-5	Rank-1	Rank-5	Rank-1	Rank-5
LR face	22.96%	25.70%	22.96%	25.70%	15.82%	27.07%	15.82%	27.07%	70.09%	76.33%	57.26%	63.17%
TANN [7]	35.72%	40.32%	30.55%	34.09%	18.43%	32.01%	17.57%	30.61%	81.32%	85.59%	78.94%	82.60%
Vivid-GAN	47.16%	56.04%	45.57%	51.82%	19.65%	35.42%	18.54%	33.40%	85.65%	90.13%	82.18%	86.32%

“32 × 32, 4×”: 32 × 32 means the resolution of the original non-frontal LR face; 4× means the magnification factor.

F. Efficiency Analysis

We also conduct comparisons to verify the efficiency of our model. As indicated in Tab. IV, compared with “F+SR” and “SR+F” methods, our VividGAN requires relatively shorter running time because VividGAN performs face SR and frontalization seamlessly. Here, “F+SR” and “SR+F” methods adopt the work [5] for face frontalization. Due to the coarse-to-fine mechanism, VividGAN is less efficient than TANN, and the parameter capacity of VividGAN is also slightly overweight than TANN. However, we achieve much better improvements on quantitative performance, as indicated in Tab. IV. As obtaining more authentic HR faces is more important for face hallucination approaches, the trade-off between hallucination performance and model complexity in our VividGAN is acceptable.

VI. FACE HALLUCINATION EVALUATION VIA DOWNSTREAM TASKS

A. Comparisons with SOTA on Face Recognition

First of all, we demonstrate that our VividGAN boosts the performance of low resolution face recognition. We adopt the “recognition via hallucination” framework to conduct face recognition experiments on both under-controlled and unconstrained databases (see Tab. V). Concretely, aggressively downsampled or in-the-wild LR faces are first hallucinated by face hallucination methods and then used for recognition.

1) *Databases*: We partition **Multi-PIE** [59], **MMI** [60] and **CelebA** [61] databases into subject disjoint training and testing sets. We also train the compared face hallucination methods and then conduct face recognition experiments on the testing set. Tab. V manifests the detailed structure as well as the experimental protocol for each database. In our face recognition experiments, one frontal image with natural illumination and neutral expression is used as the gallery image for each testing identity. Meanwhile, the probe set is made of non-frontal LR face images.

For the in-the-wild setting, we train the face hallucination methods on CelebA, and then test on TinyFace [68], DroneSURF [68] and IJB-C [70] databases. **TinyFace** [68] is a face database established specifically for native low resolution face recognition tasks. We use their evaluation protocol and

released testing set. **DroneSURF** is the first database proposed for research of drone based face recognition. Following the original paper [68], we adopt the frame-wise identification protocol, and use the alternative frame selection technique to construct the testing set. Here, we select the frames in surveillance scenarios. **IARPA Janus Benchmark-C face challenge (IJB-C)** [70] is a challenging in-the-wild face recognition database. We employ the 1:N identification protocol, and follow the predefined multi-image face templates to generate LR probe/HR gallery face pairs. Thus, our testing setting is more challenging.

2) *Experimental Settings*: For all the testing images, we crop the face regions, resize them to 128 × 128 pixels, and thus generate our HR face images. For Multi-PIE, MMI, CelebA and IJB-C databases, we generate the non-frontal LR faces (16 × 16 or 32 × 32 pixels) by transforming and downsampling the non-frontal HR ones. As the face images in TinyFace and DroneSURF databases are captured in real-life low resolution condition, we employ them as LR images directly. Then, we employ a state-of-the-art pretrained face recognition model (SphereFaceNet [71]) to conduct face recognition experiments on LR faces and hallucinated HR faces from LR ones by different methods. We compute the cosine distance of the extracted deep features for face recognition. In particular, we train a CycleGAN [72] to alleviate the domain gap between gallery faces and hallucinated ones.

3) *Evaluation*: The performance comparisons of VividGAN and other face hallucination methods on both under-controlled and unconstrained databases are shown in Tab. VI. We take the rank-1 and rank-5 recognition rates as the evaluation metrics. As indicated by Tab. VI, the face recognition rates of our hallucinated frontal HR faces are superior to those of the non-frontal LR faces and TANN’s results on all databases. This demonstrates that our VividGAN achieves remarkable identity preservation ability and the promising potential on challenging real-world identification problems, such as drone-based face recognition, video surveillance face recognition, etc.

B. Comparisons with SOTA on Face Expression Classification

In this section, we manifest that our VividGAN also benefits low-resolution face expression classification tasks.

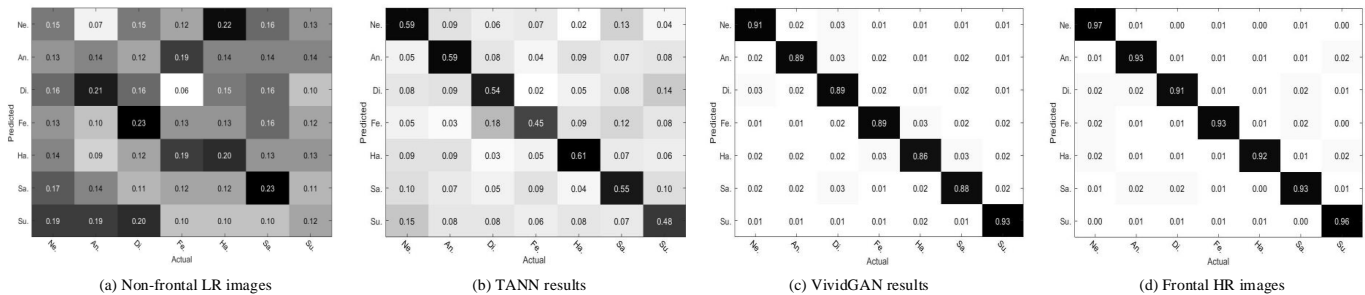


Fig. 14: The confusion matrices between the true labels and different predicted labels on the MMI database.

1) *Experimental Settings:* We perform a standard 10-fold subject-independent cross-validation [73], [74] on the MMI database. First, the synthesized frontal/non-frontal MMI face pairs are split into 10 subsets according to the identity information and the individuals in any two subsets are mutually exclusive. In each experiment, 9 subsets are used for training and the remaining one subset for testing. We train all the compared hallucination models on the same training dataset and employ a state-of-the-art expression classification model, VGG-VD-16 [75] to identify the facial expression of HR faces hallucinated from non-frontal LR ones. Here, state-of-the-art face hallucination methods are used to upsample the testing faces, while the classification results of the non-frontal LR faces upscaled by bicubic interpolation and the ground-truth frontal HR faces are also provided as baselines. At last, the expression classification performance for each method are obtained by averaging the results of the 10 folds, as indicated in Tab. VI.

2) *Evaluation:* As implied in Tab. VI, the hallucinated face images of our VividGAN are more authentic to the ground-truth frontal HR faces in comparison to the state-of-the-art, thus leading to superior face expression classification rates. Particularly, the face expression classification rate of our hallucinated faces exceeds that of the input LR ones by a large margin of 65.07%. Fig. 14 illustrates the corresponding confusion matrices. These matrices indicate that VividGAN recovers photo-realistic facial details more faithfully, and is more practical for the low resolution face expression classification task.

TABLE VII: Facial expression classification results for different methods on the MMI database

SR method	Accuracy	
	F+SR	SR+F
Bicubic	26.08%	27.95%
SRGAN [65]	31.26%	33.02%
CBN [8]	29.30%	30.17%
WaveletSRnet [33]	35.58%	37.34%
TDAE [32]	34.72%	35.69%
TANN [7]	56.70%	
Non-frontal LR	23.46%	
Frontal HR	94.62%	
VividGAN	88.53%	

C. User Study

We conduct a user study to further demonstrate the effectiveness and superiority of VividGAN. Specifically, we choose fifty female and fifty male LR faces under various poses from CelebA as our testing samples. For each testing sample, six different hallucinated HR frontal face images are shown at the same time to a user, of which one is generated by VividGAN and others are generated by the competing methods, i.e., TANN [7] and other four combination methods. Each participant is required to choose the most similar one with respect to the ground-truth image. We invite twenty participants to accomplish our user study. After the voting, we collect 2000 votes from the participants and show the percentage of votes for each compared method in Fig. 15. The result shows that the hallucinated faces obtained by our VividGAN are more favored than other methods.

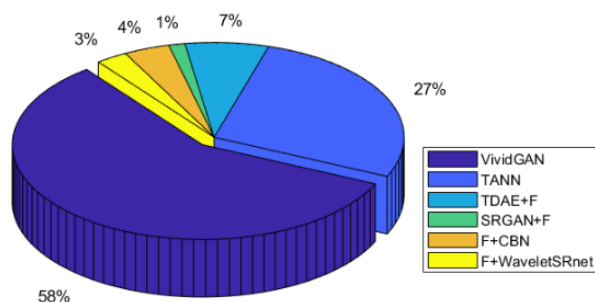


Fig. 15: User study. Results of our VividGAN and other state-of-the-art methods on CelebA faces.

VII. CONCLUSION

This paper lodges an innovative “preview” and “revise” mechanism to hallucinate a face blueprint and touch up this blueprint for enriching its HR facial details. Specifically, we present an end-to-end trainable VividGAN framework to streamline the two processes, hallucination and frontalization on tiny non-frontal face images, in a coarse-to-fine fashion. Moreover, to compensate for the obscure details in vital facial components, we also provide a solution to recovering vivid and fine-grained facial components directly from non-frontal LR faces. VividGAN fully utilizes the facial prior knowledge and achieves face SR (an upscaling factor of 8×) along with frontalization (with pose variations up to 90°). Experimental results validate the effectiveness of VividGAN,

which yields identity-preserving faces and substantially boosts the performance of downstream tasks, *i.e.*, face recognition and expression classification.

ACKNOWLEDGMENT

This work was supported by the National Natural Science Foundation of China (No.61871123) and Key Research and Development Program in Jiangsu Province (No.BE2016739). This work was supported in part by ARC under Grant DP180100106 and DP200101328.

REFERENCES

- [1] W. Zhao, R. Chellappa, P. J. Phillips, and A. Rosenfeld, "Face recognition: A literature survey," *ACM computing surveys (CSUR)*, vol. 35, no. 4, pp. 399–458, 2003.
- [2] P. Liu, Y. Lin, Z. Meng, W. Deng, J. T. Zhou, and Y. Yang, "Point adversarial self mining: A simple method for facial expression recognition in the wild," *arXiv preprint arXiv:2008.11401*, 2020.
- [3] P. Liu, Y. Wei, Z. Meng, W. Deng, J. T. Zhou, and Y. Yang, "Omnisupervised facial expression recognition: A simple baseline," *arXiv preprint arXiv:2005.08551*, 2020.
- [4] X. Yu, B. Fernando, B. Ghanem, F. Porikli, and R. Hartley, "Face super-resolution guided by facial component heatmaps," in *Proceedings of European Conference on Computer Vision (ECCV)*, 2018, pp. 217–233.
- [5] L. Q. Tran, X. Yin, and X. Liu, "Representation learning by rotating your faces," *IEEE Transactions on Pattern Analysis and Machine Intelligence*, 2018.
- [6] M. Jaderberg, K. Simonyan, A. Zisserman *et al.*, "Spatial transformer networks," in *Advances in Neural Information Processing Systems (NIPS)*, 2015, pp. 2017–2025.
- [7] X. Yu, F. Shiri, B. Ghanem, and F. Porikli, "Can we see more? joint frontalization and hallucination of unaligned tiny faces," *IEEE Transactions on Pattern Analysis and Machine Intelligence*, vol. 42, no. 9, pp. 2148–2164, 2019.
- [8] S. Zhu, S. Liu, C. C. Loy, and X. Tang, "Deep cascaded bi-network for face hallucination," in *Proceedings of European Conference on Computer Vision (ECCV)*, 2016, pp. 614–630.
- [9] Q. Cao, L. Lin, Y. Shi, X. Liang, and G. Li, "Attention-aware face hallucination via deep reinforcement learning," in *Proceedings of the IEEE Conference on Computer Vision and Pattern Recognition (CVPR)*, 2017, pp. 690–698.
- [10] Y. Chen, Y. Tai, X. Liu, C. Shen, and J. Yang, "Fsrnet: End-to-end learning face super-resolution with facial priors," in *Proceedings of the IEEE Conference on Computer Vision and Pattern Recognition (CVPR)*, 2018, pp. 2492–2501.
- [11] X. Yu and F. Porikli, "Imagining the unimaginable faces by deconvolutional networks," *IEEE Transactions on Image Processing*, vol. 27, no. 6, pp. 2747–2761, 2018.
- [12] J. Thies, M. Zollhofer, M. Stamminger, C. Theobalt, and M. Nießner, "Face2face: Real-time face capture and reenactment of rgb videos," in *Proceedings of the IEEE Conference on Computer Vision and Pattern Recognition (CVPR)*, 2016, pp. 2387–2395.
- [13] C. Sagonas, Y. Panagakis, S. Zafeiriou, and M. Pantic, "Robust statistical face frontalization," in *Proceedings of the IEEE Conference on Computer Vision and Pattern Recognition (CVPR)*, 2015, pp. 3871–3879.
- [14] T. Hassner, S. Harel, E. Paz, and R. Enbar, "Effective face frontalization in unconstrained images," in *Proceedings of the IEEE Conference on Computer Vision and Pattern Recognition (CVPR)*, 2015, pp. 4295–4304.
- [15] R. Huang, S. Zhang, T. Li, and R. He, "Beyond face rotation: Global and local perception gan for photorealistic and identity preserving frontal view synthesis," in *Proceedings of International Conference on Computer Vision (ICCV)*, 2017, pp. 2439–2448.
- [16] V. Blanz, T. Vetter *et al.*, "A morphable model for the synthesis of 3d faces," in *Siggraph*, vol. 99, 1999, pp. 187–194.
- [17] X. Zhu, Z. Lei, J. Yan, D. Yi, and S. Z. Li, "High-fidelity pose and expression normalization for face recognition in the wild," in *Proceedings of the IEEE Conference on Computer Vision and Pattern Recognition (CVPR)*, 2015, pp. 787–796.
- [18] X. Yu, F. Porikli, B. Fernando, and R. Hartley, "Hallucinating unaligned face images by multiscale transformative discriminative networks," *International Journal of Computer Vision*, pp. 1–27, 2019.
- [19] X. Yu, B. Fernando, R. Hartley, and F. Porikli, "Super-resolving very low-resolution face images with supplementary attributes," in *Proceedings of the IEEE Conference on Computer Vision and Pattern Recognition (CVPR)*, 2018, pp. 908–917.
- [20] X. Yu, F. Porikli, B. Fernando, and R. Hartley, "Hallucinating unaligned face images by multiscale transformative discriminative networks," *International Journal of Computer Vision*, vol. 128, no. 2, pp. 500–526, 2020.
- [21] X. Yu, B. Fernando, R. Hartley, and F. Porikli, "Semantic face hallucination: Super-resolving very low-resolution face images with supplementary attributes," *IEEE transactions on pattern analysis and machine intelligence*, 2019.
- [22] X. Wang and X. Tang, "Hallucinating face by eigentransformation," *IEEE Transactions on Systems, Man, and Cybernetics, Part C (Applications and Reviews)*, vol. 35, no. 3, pp. 425–434, 2005.
- [23] C. Liu, H.-Y. Shum, and W. T. Freeman, "Face hallucination: Theory and practice," *International Journal of Computer Vision*, vol. 75, no. 1, pp. 115–134, 2007.
- [24] S. Kolouri and G. K. Rohde, "Transport-based single frame super resolution of very low resolution face images," in *Proceedings of the IEEE Conference on Computer Vision and Pattern Recognition (CVPR)*, 2015, pp. 4876–4884.
- [25] X. Ma, J. Zhang, and C. Qi, "Hallucinating face by position-patch," *Pattern Recognition*, vol. 43, no. 6, pp. 2224–2236, 2010.
- [26] R. A. Farrugia and C. Guillemot, "Face hallucination using linear models of coupled sparse support," *IEEE Transactions on Image Processing*, vol. 26, no. 9, pp. 4562–4577, 2017.
- [27] J. Jiang, R. Hu, Z. Wang, and Z. Han, "Face super-resolution via multi-layer locality-constrained iterative neighbor embedding and intermediate dictionary learning," *IEEE Transactions on Image Processing*, vol. 23, no. 10, pp. 4220–4231, 2014.
- [28] L. Liu, C. P. Chen, S. Li, Y. Y. Tang, and L. Chen, "Robust face hallucination via locality-constrained bi-layer representation," *IEEE Transactions on Cybernetics*, vol. 48, no. 4, pp. 1189–1201, 2017.
- [29] M. F. Tappen and C. Liu, "A bayesian approach to alignment-based image hallucination," in *Proceedings of European Conference on Computer Vision (ECCV)*, 2012, pp. 236–249.
- [30] C.-Y. Yang, S. Liu, and M.-H. Yang, "Hallucinating compressed face images," *International Journal of Computer Vision*, vol. 126, no. 6, pp. 597–614, 2018.
- [31] X. Yu and F. Porikli, "Ultra-resolving face images by discriminative generative networks," in *Proceedings of European Conference on Computer Vision (ECCV)*, 2016, pp. 318–333.
- [32] —, "Face hallucination with tiny unaligned images by transformative discriminative neural networks," in *Thirty-First AAAI Conference on Artificial Intelligence*, 2017, p. 4327–4333.
- [33] H. Huang, R. He, Z. Sun, and T. Tan, "Wavelet domain generative adversarial network for multi-scale face hallucination," *International Journal of Computer Vision*, vol. 127, no. 6-7, pp. 763–784, 2019.
- [34] X. Xu, D. Sun, J. Pan, Y. Zhang, H. Pfister, and M.-H. Yang, "Learning to super-resolve blurry face and text images," in *Proceedings of International Conference on Computer Vision (ICCV)*, 2017, pp. 251–260.
- [35] R. Dahl, M. Norouzi, and J. Shlens, "Pixel recursive super resolution," in *Proceedings of International Conference on Computer Vision (ICCV)*, 2017, pp. 5439–5448.
- [36] A. V. Oord, N. Kalchbrenner, and K. Kavukcuoglu, "Pixel recurrent neural networks," in *Proceedings of Machine Learning Research*, vol. 48, 2016, pp. 1747–1756.
- [37] Y. Zhang, I. W. Tsang, Y. Luo, C.-H. Hu, X. Lu, and X. Yu, "Copy and paste gan: Face hallucination from shaded thumbnails," in *Proceedings of the IEEE Conference on Computer Vision and Pattern Recognition (CVPR)*, 2020, pp. 7355–7364.
- [38] A. Bulat, J. Yang, and G. Tzimiropoulos, "To learn image super-resolution, use a gan to learn how to do image degradation first," in *Proceedings of European Conference on Computer Vision (ECCV)*, 2018, pp. 185–200.
- [39] F. Yang, J. Wang, E. Shechtman, L. Bourdev, and D. Metaxas, "Expression flow for 3d-aware face component transfer," *ACM Transactions on Graphics*, vol. 30, no. 4, p. 60, 2011.
- [40] D. Jiang, Y. Hu, S. Yan, L. Zhang, H. Zhang, and W. Gao, "Efficient 3d reconstruction for face recognition," *Pattern Recognition*, vol. 38, no. 6, pp. 787–798, 2005.
- [41] A. Asthana, T. K. Marks, M. J. Jones, K. H. Tieu, and M. Rohith, "Fully automatic pose-invariant face recognition via 3d pose normalization," in *Proceedings of International Conference on Computer Vision (ICCV)*, IEEE, 2011, pp. 937–944.

- [42] T. Hassner, "Viewing real-world faces in 3d," in *Proceedings of International Conference on Computer Vision (ICCV)*, 2013, pp. 3607–3614.
- [43] Y. Taigman, M. Yang, M. Ranzato, and L. Wolf, "Deepface: Closing the gap to human-level performance in face verification," in *Proceedings of the IEEE Conference on Computer Vision and Pattern Recognition (CVPR)*, 2014, pp. 1701–1708.
- [44] I. Masi, A. T. Tran, T. Hassner, J. T. Leksut, and Medioni, "Do we really need to collect millions of faces for effective face recognition?" in *Proceedings of European Conference on Computer Vision (ECCV)*. Springer, 2016, pp. 579–596.
- [45] V. Blanz and T. Vetter, "Face recognition based on fitting a 3d morphable model," *IEEE Transactions on Pattern Analysis and Machine Intelligence*, vol. 25, no. 9, pp. 1063–1074, 2003.
- [46] Z. Zhu, P. Luo, X. Wang, and X. Tang, "Recover canonical-view faces in the wild with deep neural networks," *arXiv preprint arXiv:1404.3543*, 2014.
- [47] J. Yim, H. Jung, B. Yoo, C. Choi, D. Park, and J. Kim, "Rotating your face using multi-task deep neural network," in *Proceedings of the IEEE Conference on Computer Vision and Pattern Recognition (CVPR)*, 2015, pp. 676–684.
- [48] F. Cole, D. Belanger, D. Krishnan, A. Sarna, I. Mosseri, and W. T. Freeman, "Synthesizing normalized faces from facial identity features," in *Proceedings of the IEEE Conference on Computer Vision and Pattern Recognition (CVPR)*, 2017, pp. 3703–3712.
- [49] Y. Hu, X. Wu, B. Yu, R. He, and Z. Sun, "Pose-guided photorealistic face rotation," in *Proceedings of the IEEE Conference on Computer Vision and Pattern Recognition (CVPR)*, 2018, pp. 8398–8406.
- [50] J. Zhao, J. Li, X. Tu, F. Zhao, Y. Xin, J. Xing, H. Liu, S. Yan, and J. Feng, "Multi-prototype networks for unconstrained set-based face recognition," in *Proceedings of the Twenty-Eighth International Joint Conference on Artificial Intelligence (IJCAI)*, 7 2019, pp. 4397–4403.
- [51] M. Kan, S. Shan, H. Chang, and X. Chen, "Stacked progressive auto-encoders (spae) for face recognition across poses," in *Proceedings of the IEEE Conference on Computer Vision and Pattern Recognition (CVPR)*, 2014, pp. 1883–1890.
- [52] A. Tuan Tran, T. Hassner, I. Masi, and G. Medioni, "Regressing robust and discriminative 3d morphable models with a very deep neural network," in *Proceedings of the IEEE Conference on Computer Vision and Pattern Recognition (CVPR)*, 2017, pp. 5163–5172.
- [53] I. Goodfellow, J. Pouget-Abadie, M. Mirza, B. Xu, D. Warde-Farley, S. Ozair, A. Courville, and Y. Bengio, "Generative adversarial nets," in *Advances in Neural Information Processing Systems (NIPS)*, 2014, pp. 2672–2680.
- [54] J. Cao, Y. Hu, H. Zhang, R. He, and Z. Sun, "Towards high fidelity face frontalization in the wild," *International Journal of Computer Vision*, pp. 1–20, 2019.
- [55] K. He, X. Zhang, S. Ren, and J. Sun, "Deep residual learning for image recognition," in *Proceedings of the IEEE Conference on Computer Vision and Pattern Recognition (CVPR)*, 2016, pp. 770–778.
- [56] J. Johnson, A. Alahi, and L. Fei-Fei, "Perceptual losses for real-time style transfer and super-resolution," in *European conference on computer vision*. Springer, 2016, pp. 694–711.
- [57] A. Bulat and G. Tzimiropoulos, "Super-fan: Integrated facial landmark localization and super-resolution of real-world low resolution faces in arbitrary poses with gans," in *Proceedings of the IEEE Conference on Computer Vision and Pattern Recognition (CVPR)*, June 2018.
- [58] C. Chen, Q. Chen, J. Xu, and V. Koltun, "Learning to see in the dark," in *Proceedings of the IEEE Conference on Computer Vision and Pattern Recognition (CVPR)*, 2018, pp. 3291–3300.
- [59] R. Gross, I. Matthews, J. Cohn, T. Kanade, and S. Baker, "Multi-pie," *Image and Vision Computing*, vol. 28, no. 5, pp. 807–813, 2010.
- [60] M. F. Valstar and M. Pantic, "Induced disgust, happiness and surprise: an addition to the mmi facial expression database," in *Proceedings of International Conference on Language Resources and Evaluation, Workshop on EMOTION*, Malta, May 2010, pp. 65–70.
- [61] Z. Liu, P. Luo, X. Wang, and X. Tang, "Deep learning face attributes in the wild," in *Proceedings of International Conference on Computer Vision (ICCV)*, December 2015, p. 3730–3738.
- [62] Y. Zhang, P. Lv, X. Lu, and J. Li, "Face detection and alignment method for driver on highroad based on improved multi-task cascaded convolutional networks," *Multimedia Tools and Applications*, pp. 1–19, 2019.
- [63] A. Newell, K. Yang, and J. Deng, "Stacked hourglass networks for human pose estimation," in *Proceedings of European Conference on Computer Vision (ECCV)*, 2016, pp. 483–499.
- [64] F. Shiri, X. Yu, F. Porikli, R. Hartley, and P. Koniusz, "Recovering faces from portraits with auxiliary facial attributes," in *2019 IEEE Winter Conference on Applications of Computer Vision (WACV)*. IEEE, 2019, pp. 406–415.
- [65] C. Ledig, L. Theis, F. Huszár, J. Caballero, A. Cunningham, A. Acosta, A. Aitken, A. Tejani, J. Totz, Z. Wang *et al.*, "Photo-realistic single image super-resolution using a generative adversarial network," in *Proceedings of the IEEE Conference on Computer Vision and Pattern Recognition (CVPR)*, 2017, pp. 4681–4690.
- [66] F. Shiri, X. Yu, F. Porikli, R. Hartley, and P. Koniusz, "Identity-preserving face recovery from stylized portraits," *International Journal of Computer Vision*, vol. 127, no. 6-7, pp. 863–883, 2019.
- [67] A. Bulat and G. Tzimiropoulos, "How far are we from solving the 2d & 3d face alignment problem?(and a dataset of 230,000 3d facial landmarks)," in *Proceedings of International Conference on Computer Vision (ICCV)*, 2017, pp. 1021–1030.
- [68] Z. Cheng, X. Zhu, and S. Gong, "Low-resolution face recognition," in *Asian Conference on Computer Vision*. Springer, 2018, pp. 605–621.
- [69] I. Kalra, M. Singh, S. Nagpal, R. Singh, M. Vatsa, and P. Sujit, "Dronesurf: Benchmark dataset for drone-based face recognition," in *2019 14th IEEE International Conference on Automatic Face & Gesture Recognition (FG 2019)*. IEEE, 2019, pp. 1–7.
- [70] B. Maze, J. Adams, J. A. Duncan, N. Kalka, T. Miller, C. Otto, A. K. Jain, W. T. Niggel, J. Anderson, J. Cheney *et al.*, "Iarpa janus benchmark-c: Face dataset and protocol," in *Proceedings of International Conference on Biometrics (ICB)*, 2018, pp. 158–165.
- [71] W. Liu, Y. Wen, Z. Yu, M. Li, B. Raj, and L. Song, "Sphereface: Deep hypersphere embedding for face recognition," in *Proceedings of the IEEE Conference on Computer Vision and Pattern Recognition (CVPR)*, 2017.
- [72] J.-Y. Zhu, T. Park, P. Isola, and A. A. Efros, "Unpaired image-to-image translation using cycle-consistent adversarial networks," in *Proceedings of the IEEE Conference on Computer Vision and Pattern Recognition (CVPR)*, 2017, pp. 2223–2232.
- [73] P. Liu, S. Han, Z. Meng, and Y. Tong, "Facial expression recognition via a boosted deep belief network," in *Proceedings of the IEEE Conference on Computer Vision and Pattern Recognition (CVPR)*, 2014, pp. 1805–1812.
- [74] P. Liu, J. T. Zhou, I. W.-H. Tsang, Z. Meng, S. Han, and Y. Tong, "Feature disentangling machine—a novel approach of feature selection and disentangling in facial expression analysis," in *Proceedings of European Conference on Computer Vision (ECCV)*. Springer, 2014, pp. 151–166.
- [75] K. Simonyan and A. Zisserman, "Very deep convolutional networks for large-scale image recognition," in *Proceedings of International Conference on Learning Representations (ICLR)*, 2015, pp. 1–14.